Available online at www.sciencedirect.com

SciVerse ScienceDirect

journal homepage: www.elsevier.com/locate/he

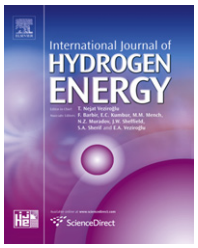

Hydrogen permeation and diffusion in densified MOF-5 pellets

C. Xu [a,*], J. Yang [a,*], M. Veenstra [a], A. Sudik [a], J.J. Purewal [b], Yang Ming [b], B.J. Hardy [c], J. Warner [a], S. Maurer [d], U. Müeller [d], Donald J. Siegel [b]

[a] Ford Motor Company, Research and Advanced Engineering, MD 1170/RIC, Dearborn MI 48121, USA
[b] Department of Mechanical Engineering, University of Michigan, 2350 Hayward St., Ann Arbor, MI 28190, USA
[c] Savannah River National Laboratory, US Department of Energy, Aiken, SC 29808, USA
[d] BASF SE Chemicals Research and Engineering, 67056 Ludwigshafen, Germany

ARTICLE INFO

Article history:
Received 25 May 2012
Received in revised form
10 December 2012
Accepted 18 December 2012
Available online 30 January 2013

Keywords:
Hydrogen storage
MOF-5
Pressure drop
Steady flow state
Darcy permeability
Fick diffusion

ABSTRACT

The metal-organic framework $Zn_4O(BDC)_3$ (BDC = 1,4-bezene dicarboxlate), also known as MOF-5, has demonstrated considerable adsorption of hydrogen, up to 7 excess wt.% at 77 K. Consequently, it has attracted significant attention for vehicular hydrogen storage applications. To improve the volumetric hydrogen density and thermal conductivity of MOF-5, prior studies have examined the hydrogen storage capacities of dense MOF-5 pellets and the impact of thermally conductive additives such as expanded natural graphite (ENG). However, the performance of a storage system based on densified MOF-5 powders will also hinge upon the rate of hydrogen mass transport through the storage medium. In this study, we further characterize MOF-5 compacts by measuring their hydrogen transport properties as a function of pellet density (ρ = 0.3–0.5 g cm^{-3}) and the presence/absence of ENG additions. More specifically, the Darcy permeability and diffusivity of hydrogen in pellets of neat MOF-5, and composite pellets consisting of MOF-5 with 5 and 10 wt.% ENG additions, have been measured at ambient (296 K) and liquid nitrogen (77 K) temperatures. The experimental data suggest that the H_2 transport in densified MOF-5 is strongly related to the MOF-5 pellet density ρ.

1. Introduction

MOFs have been studied for gas storage and separation applications for more than three decades [1,2]. MOF-5 is a highly porous, crystalline solid constructed from a periodic array of metal clusters linked through multi-topic organic struts [3,4]. In particular, frameworks consisting of tetrahedral $[Zn_4O]^{6+}$ units connected via rigid multi-topic carboxylate linkers have been shown to adsorb large amounts of hydrogen reversibly at low temperature and moderate pressure [3,5,6]. However, MOF-5 powders have low density and poor thermal conductivity, which are major drawbacks from an engineering perspective. By mechanical compaction, MOF powders can be converted into pellets with higher densities [7], which have been shown to improve volumetric hydrogen storage densities with minor losses in gravimetric density. The thermal conductivity of MOF-5 pellets can be enhanced by mixing MOF-5 powders with Expanded Natural Graphite (ENG) [8]. Our studies [8,9] have found that improved hydrogen storage properties are achieved for pellet densities of 0.5 g cm^{-3},

* *Corresponding authors.*
E-mail addresses: cxu22@ford.com (C. Xu), jyang27@ford.com (J. Yang).
0360-3199/$ – see front matter
http://dx.doi.org/10.1016/j.ijhydene.2012.12.096

yielding a 350% increase in volumetric H_2 density with only a modest 15 ~ 20% reduction in gravimetric H_2 excess in comparison to the powder. Higher pellet densities result in larger reductions in gravimetric excess capacity [8,9] and negatively affect the crystal structure when pellet density approaches single crystal density [10]. ENG additions of 5 ~ 10 wt.% are found to improve thermal conductivity while preserving the hydrogen volumetric and reducing the gravimetric capacities by only 20% or 30% when the pellet densities are ~0.5 g cm^{-3} [8]. In this paper, we studied the hydrogen mass transfer properties, the H_2 permeability and diffusivity, which characterize H_2 charge and discharge dynamics in MOF-5 and MOF-5/ENG composite, as a function of the density of compressed pellets.

2. Experimental methods

2.1. Sample preparation and test setup

The preparation methods for MOF-5 powder have been described previously [11]. Expanded natural graphite (ENG) worms were supplied by SGL Group. MOF-5 powders were mixed with ENG worms using a Spex 8000 Mixer/Mill with ENG contents of 5 and 10 wt.% for 20 s without the mixing balls. The loading of the mixture into the milling vial is performed in an Ar filled MBraun Labmaster 130 glove box with O_2 and H_2O content of less than 1 ppm. After mixing, the powder is pressed into pellets of different densities inside the glove box using a REFLEX Analytical's bench top Pellet Press. The neat MOF-5 and MOF-5/ENG mixtures were loaded into a cylindrical die with a 1.27 cm diameter. Pellets of different bulk densities were obtained by controlling the mass of the MOF-5 mixture and applying different pressing forces. Bulk densities were calculated from the mass and physical dimensions of each pellet. Based on hydrogen density and thermal conductivity measurement, the pellet densities ρ were controlled to be between 0.3 and 0.5 g cm^{-3}.

The H_2 permeability measurement setup is shown in Fig. 1a. A cylindrical pellet was secured in the sample holder using silicone adhesive sealant sealing around the sample edge in the glove box. The effective gas flow diameter d was 1.00 cm, and the sample thickness h was 0.5 cm (Fig. 1b). Two pressure transducers P_1 and P_2 (OMEGA PX-240A) were connected adjacent to the sample holder in upstream and downstream positions, respectively. A thermocouple was positioned downstream about 5 mm near the sample to measure the gas temperature. Since the thermocouple is positioned close to the sample, we assume that the measured temperature reflects the temperature of the sample. The temperature, H_2 inlet and outlet pressure were recorded by a data acquisition module (DAQ: OMEGA OM-DAQ-USB-2401).

For the cryogenic H_2 transport measurements at 77 K, the sample holder (see Fig. 1a) was completely submerged in a liquid N_2 (LN) Dewar, and the liquid N_2 level was kept constant. MOF-5 has a negative thermal-expansion coefficient which helps to secure the seal between the sample and the sample holder [12,13]. H_2 gas flowed through 1/4 inch stainless steel tubing and then through copper coil within the liquid N_2 Dewar to ensure that the H_2 gas was cooled down to 77 K before flowing through the sample. The measured H_2 outlet temperature was between 77 and 79 K upon exiting the copper tube with a flow rate of up to 550 standard cubic centimeters per minute (sccm), which was the maximum flow rate used in this study. For the measurements at 296 K, the pressure drop was taken without using LN.

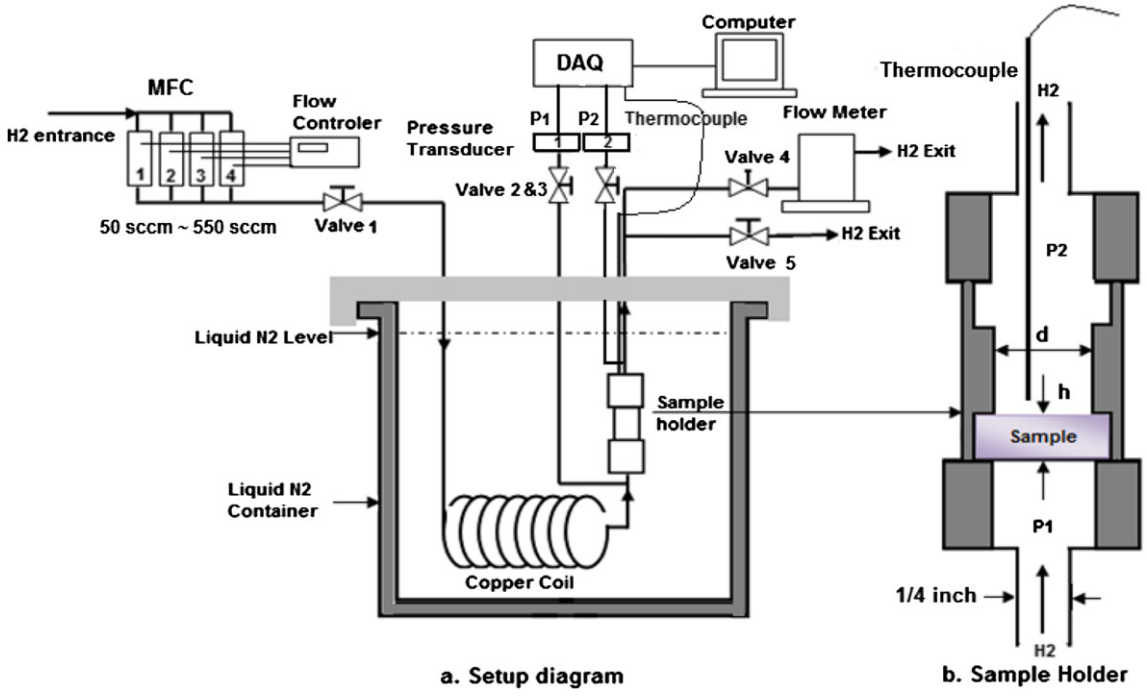

Fig. 1 – Diagram of the H_2 permeability measurement apparatus.

The measurement set-up had four mass flow meters (MSK) which were set at H_2 flow rates of 50 sccm, 100 sccm, 200 sccm and 200 sccm to create a H_2 flow rate from 0 sccm to 550 sccm. A bubble flow meter was connected to the H_2 exit to confirm the flow rate. At steady state, the H_2 inlet pressure P_1 and outlet pressure P_2 are constant. P_2 is very close to the ambient pressure between 745 and 755 torr, as read from a barometer. $\Delta P = P_1 - P_2$ is the measured pressure drop when H_2 flows through the sample. The steady flow is reached when the inlet flow rate equals outlet flow rate. For each sample, 11 pressure-drops corresponding to 11 flow rates from 50 sccm to 550 sccm at 50 sccm increments were measured. The H_2 flow was allowed to reach steady state at each step. In order to evaluate the effects of degassing on permeability, some samples were degassed at 130 °C using heating tape attached to the sample holder and a mechanical pump connected through the H_2 exit. The valves 1 to 5 were used to control H_2 flow and prevent air from leaking into the sample holder during degassing and subsequent cooling down.

2.2. Darcy permeability

For a comparison analysis, the Darcy permeability was calculated using two approaches by assuming H_2 gas as incompressible and compressible.

For incompressible H_2 gas, Darcy permeability is given by the Darcy equation:

$$\kappa = \frac{v\mu h}{\Delta P} \tag{1}$$

where v is the H_2 flow velocity through the sample, μ is the H_2 viscosity [14], h is the sample thickness, and $\Delta P = P_1 - P_2$ is the pressure drop between inlet and outlet pressure under steady flow.

When assuming H_2 gas as a compressible ideal gas, the pressure drop is given by [15]:

$$\Delta P = \frac{P_1^2 - P_2^2}{2P_2}$$

In this case, the Darcy equation is given by:

$$\kappa = \frac{2P_2}{(P_1^2 - P_2^2)} v\mu h \tag{2}$$

Therefore, by measuring the pressure drop and flow rate, the Darcy permeability for H_2 as an incompressible and compressible gas can be calculated using Eqs. (1) and (2), respectively. In both cases, the Darcy permeability was calculated as a function of sample density, ENG content (neat, 5% or 10%), and temperature (296 or 77 K).

2.3. Diffusivity and H_2 concentration

The diffusivity of H_2 in MOF-5 pellets under steady flow conditions was calculated using the one dimensional (1-D) Fick's first law:

$$J = -D_f \frac{\Delta C}{\Delta x}. \tag{3}$$

Here D_f ($m^2\ s^{-1}$) is the Fick's diffusivity or diffusion coefficient, J (mol $m^{-2}\ s^{-1}$) is the gas mole flux per square meter at steady flow state, which is known from measured H_2 flow rate, $\Delta C/\Delta x$ is the gas concentration gradient between the two surfaces of the sample, and x (cm) is the distance away from the surface of the H_2 inlet. Using the ideal gas equation:

$$\Delta C = \frac{P_1 - P_2}{RT} = \frac{\Delta P}{RT}$$

$$\text{So } D_f = J\frac{\Delta x}{\Delta C} = \frac{JRTh}{\Delta P} \tag{4}$$

where R is the ideal gas constant 8.3145 $Jmol^{-1}\ K^{-1}$, T is gas temperature (K), C is gas concentration or density (mol m^{-3}), and Δx is the sample thickness h (m).

From the measured pressure drop at each flow rate, the diffusivity was calculated using Eq. (4). Subsequently, the H_2 concentration in the sample can be derived using Fick's second law:

$$\frac{\partial C}{\partial t} = D_f \frac{\partial^2 C}{\partial x^2} \tag{5}$$

At time $t = 0$, the initial upstream H_2 concentration at sample surface holds as constant C_1, and the downstream background H_2 concentration is C_2. For H_2 diffusion in a1-D half infinite length sample, H_2 concentration at position x (cm) away from the upstream surface and time t can be expressed as:

$$C(t,x) = C_1 - (C_1 - C_2)\mathrm{erf}\left(\frac{x}{2\sqrt{D_f t}}\right) \tag{6}$$

3. Results and discussion

3.1. Darcy permeability

Pressure drops as a function of time are plotted in Fig. 2 for a MOF-5 + 5 wt.% ENG pellet with a hydrogen flow rate from

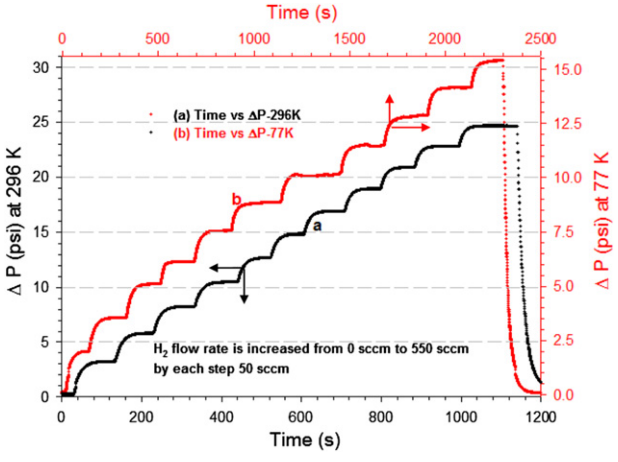

Fig. 2 – Pressure drops across a MOF-5 + 5 wt.% ENG sample (density 0.3981 g cm^{-3}) at (a) 296 K (left & bottom axis) and (b) 77 K (right & top axis) measured for increasing H_2 flow rates. The flow rate is increased from 0 to 550 sccm in 50 sccm increments during the course of the experiment.

Table 1 – MOF-5 sample density vs Darcy permeability & Fick's diffusivity.

MOF-5 at 296 K			MOF-5 at 77 K		
D (g cm^{-3})	κ, κ_c (Darcy)	D_f (m^2 s^{-1})	D (g cm^{-3})	κ, κ_c (Darcy)	D_f (m^2 s^{-1})
0.3010	0.2030, 0.1875	2.257×10^{-3}	0.3003	0.0477, 0.0456	1.339×10^{-3}
0.3110	0.1473, 0.1322	1.626×10^{-3}	0.3068	0.0406, 0.0387	1.147×10^{-3}
0.3210	0.1220, 0.1081	1.367×10^{-3}	0.3417	0.0153, 0.0138	4.330×10^{-4}
0.3417	0.0593, 0.0423	5.951×10^{-4}	0.4000	0.0040, 0.0035	1.312×10^{-4}
0.3492	0.0462, 0.0349	5.136×10^{-4}	0.4732	0.0033, 0.0024	9.587×10^{-5}
0.4013	0.0173, 0.0094	1.911×10^{-4}	0.4829	0.0026, 0.0017	7.362×10^{-5}
0.4624	0.0132, 0.0064	1.454×10^{-4}	0.4973	0.0012, 0.0006	3.589×10^{-5}
0.4732	0.0121, 0.0056	1.337×10^{-4}			
0.4904	0.0098, 0.0046	1.093×10^{-4}			

0 to 550 sccm with 50 sccm incremental steps measured at 296 K and 77 K. The equilibrium pressure drop at steady H_2 flow state was used to calculate the Darcy permeability using the incompressible gas Darcy Eq. (1), Tables 1–3 list the Darcy permeability (κ) of neat MOF-5, MOF-5 + 5 wt.% ENG and MOF-5 + 10 wt.% ENG samples of various densities. The permeability values of the samples with varying ENG content measured at 77 and 296 K versus sample density are also shown in Fig. 3. The results show H_2 permeability decreases exponentially with the density of the pellet. In addition, the permeability measured at 296 K is higher than that measured at 77 K for the same sample. At 296 K, the MOF-5 + 5 wt.% ENG sample has higher permeability than neat MOF-5 sample, and MOF-5 + 10 wt.% ENG sample has slightly higher permeability than MOF-5 + 5 wt.% ENG up to a pellet density of around 0.4 g cm^{-3}. At 77 K, the permeability of neat MOF-5, MOF-5 + 5 wt.% ENG and MOF-5 + 10 wt.% ENG samples do not differ significantly. Fig. 3 also shows that degassing does not change the H_2 permeability significantly, as indicated by the 3 open and 3 solid star data points for 77 K and 296 K, respectively.

The effects of gas compressibility on H_2 permeation were demonstrated by calculating the Darcy permeability using incompressible gas Eq. (1) and compressible ideal gas Eq. (2) for the neat MOF-5 samples. The results are plotted versus sample density in Fig. 4. At 296 K, the compressible gas Darcy permeability is 7.5% lower than the incompressible gas Darcy permeability for the low density (0.301 g cm^{-3}) sample and 52% lower than that for the high density (0.490 g cm^{-3}) sample. At 77 K, the compressible gas Darcy permeability is still smaller than the corresponding incompressible gas Darcy permeability, the difference ranges from 5% to 56% for low density pellet and high density pellet, respectively. These differences come from the fact that higher density samples lead to larger H_2 pressure drops, which result in a larger difference between compressible and incompressible gas permeability. The results of the compressible gas Darcy permeability (κ_c) for the various samples are also listed in Tables 1–3 along with the incompressible gas Darcy permeability (κ). The Darcy permeability values provide a direct comparison of H_2 permeation through MOF-5 samples with different density and ENG content at 77 K and 296 K. The results suggest that lower density samples will have better H_2 mass transport properties.

The approaches for calculating the Darcy permeability have some aspects that need to be further evaluated. The incompressible Darcy permeability approach assumes the fluid to be incompressible Newtonian fluid with a constant viscosity μ. In fact H_2 is a compressible gas, the modified compressible fluid Darcy permeability approach should give more accurate results. However, in Eq. (2), the gas viscosity μ and flow velocity v are assumed to be constant, which will lead to some error. In practical applications, the hydrogen filling pressure could be much higher, as high as 150 bar. At such high pressure, the assumptions for the Darcy permeability calculation using Eqs. (1) and (2) may not be satisfied,

Table 2 – MOF-5 + 5 wt.% ENG sample density vs Darcy permeability & Fick's diffusivity.

MOF-5 + 5% ENG at 296 K			MOF-5 +5% ENG at 77 K		
D (g cm^{-3})	κ, κ_c (Darcy)	D_f (m^2 s^{-1})	D (g cm^{-3})	κ, κ_c (Darcy)	D_f (m^2 s^{-1})
0.3057	0.1896, 0.1743	2.086×10^{-3}	0.2914	0.0486, 0.0465	1.373×10^{-3}
0.3096	0.1741, 0.1717	1.942×10^{-3}	0.3244	0.0209, 0.0193	5.877×10^{-4}
0.3244	0.0796, 0.0689	9.028×10^{-4}	0.3587	0.0081, 0.0068	2.292×10^{-4}
0.3587	0.0581, 0.0461	6.314×10^{-4}	0.3600	0.0094, 0.0081	2.671×10^{-4}
0.3981	0.0278, 0.0185	3.059×10^{-4}	0.3974	0.0044, 0.0032	1.258×10^{-4}
0.4510	0.0160, 0.0087	1.764×10^{-4}	0.3981	0.0046, 0.0036	1.321×10^{-4}
0.4908	0.0114, 0.0020	1.275×10^{-4}	0.4317	0.0041, 0.0031	1.169×10^{-4}
0.4933	0.0081, 0.0036	8.929×10^{-5}	0.4510	0.0029, 0.0020	8.314×10^{-5}
0.4942	0.0064, 0.0029	7.053×10^{-5}	0.4933	0.0026, 0.0018	7.411×10^{-5}
			0.4942	0.0022, 0.0015	5.971×10^{-5}

Table 3 – MOF-5 + 10 wt.% ENG sample density vs Darcy permeability & Fick's diffusivity.

MOF-5 + 10% ENG at 296 K			MOF-5 + 10% ENG at 77 K		
D (g cm^{-3})	κ, κ_c (Darcy)	D_f (m^2 s^{-1})	D (g cm^{-3})	κ, κ_c (Darcy)	D_f (m^2 s^{-1})
0.3008	0.2748, 0.2578	3.064×10^{-3}	0.3100	0.0534, 0.0513	1.369×10^{-3}
0.3123	0.1880, 0.1730	2.097×10^{-3}	0.3570	0.0125, 0.0111	3.528×10^{-4}
0.3477	0.0936, 0.0820	1.052×10^{-4}	0.4429	0.0036, 0.0016	1.011×10^{-4}
0.3833	0.0453, 0.0328	5.054×10^{-4}	0.5076	0.0020, 0.0012	5.591×10^{-5}
0.4054	0.0321, 0.0224	3.577×10^{-4}			
0.4429	0.0117, 0.0056	1.272×10^{-4}			
0.4952	0.0091, 0.0041	1.017×10^{-4}			

consequently, the obtained Darcy permeability data at low H_2 pressure may need to be modified for a practical storage system. Furthermore, the Darcy permeability does not fully characterize the hydrogen transport dynamics in the sample, which is needed for modeling the storage system design. H_2 diffusivity through the pellet provides additional relevant data for modeling the hydrogen transport dynamics, and will be discussed in the following section.

3.2. H_2 diffusivity

When calculating H_2 diffusivity using Fick's first law, the pressure and volume change of the H_2 gas in the sample do not affect the calculated results since the mole mass flux J (mol m^{-2} s^{-1}) is constant after H_2 flow reaches steady state. According to Eq. (4), diffusivity is inversely proportional to pressure drop across the sample ΔP. Fig. 5 shows the change in H_2 diffusivity with the pellet density for neat MOF-5, MOF-5 + 5 wt.% ENG, and MOF-5 + 10 wt.% ENG pellets at 77 K and 296 K. These results indicate that the H_2 diffusivity decreases exponentially with increasing sample density, which appears to follow a linear trend that deviates slightly at higher pellet density. This change in the diffusivity at higher densities could have been caused by the MOF-5 crystalline structure damage by compaction when pellet density approaches the single crystal density [10]. Fig. 5 also shows that the diffusivity is lower at 77 K than at 296 K, consistent with the permeability values.

Generally, the diffusivity relates to temperature and diffusion barrier (activation) by Arrhenius equation:

$$D_f = g\lambda\left(\frac{8RT}{\pi M}\right)^{\frac{1}{2}}\exp\left(-\frac{E_a}{RT}\right) \tag{7}$$

where E_a is the barrier or activation energy of the H_2 molecular transport in the sample, T is the sample temperature (K), g is the probability of forward jumping of H_2 in the direction of diffusion, M is the H_2 molecular mass, and λ is the H_2 molecular mean free path [16,17]. By assuming that the g and λ are constants at certain temperature T, the diffusivity D_f is an exponential decay of the activation energy E_a.

As shown in Fig. 5, the diffusivity changes with sample density according to an exponential decay at both 77 K and 296 K. For MOF-5 samples, the relation derived from fitting experimental data of diffusivity versus the sample density at 296 K and 77 K are

$$D_f = 25.22\exp(-31.12\cdot\text{Density}) \quad \text{for 296 K}$$

$$D_f = 8.89\exp(-29.48\cdot\text{Density}) \quad \text{for 77 K}$$

Assuming the activation energy E_a is linearly related to the sample density, the activation energy E_a was calculated using Eq. (7) and shown as linear function of pellet density in Fig. 6. Fig. 6 also shows that the H_2 diffusion activation energy at 77 K is lower than that at 296 K for a pellet with the same density, which could possibly be attributed to the slight pore volume

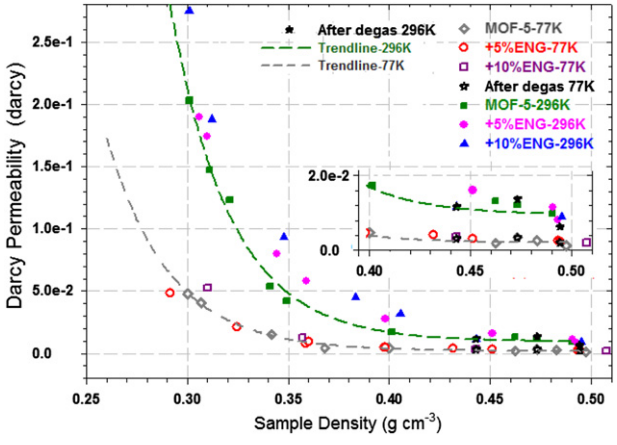

Fig. 3 – Darcy permeability of hydrogen versus sample density from the data in Tables 1–3.

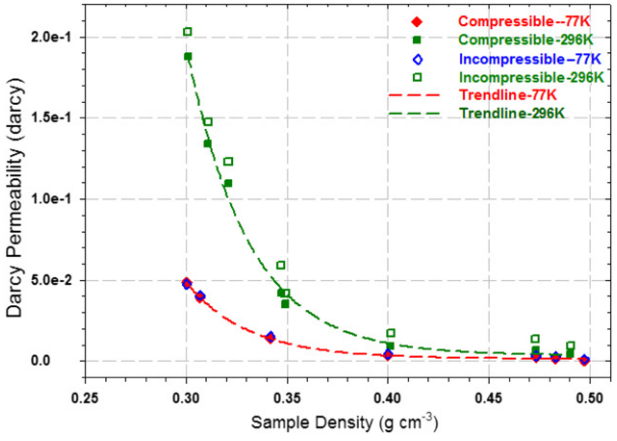

Fig. 4 – Comparison of incompressible and compressible ideal gas Darcy permeability of hydrogen for neat MOF-5 samples from the data in Table 1.

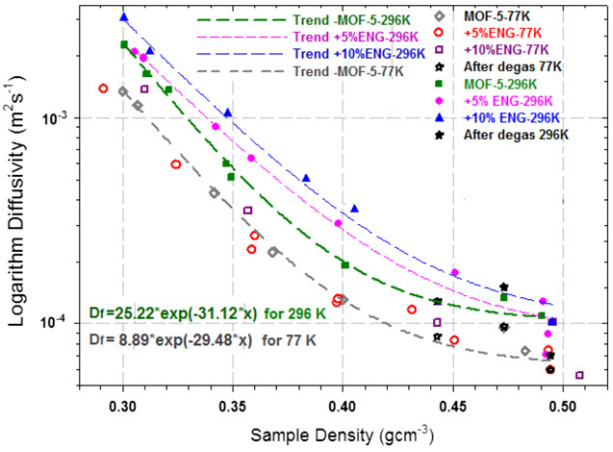

Fig. 5 – Fickian diffusivity of hydrogen with logarithmic scale versus the sample density from the diffusivity data in Tables 1–3.

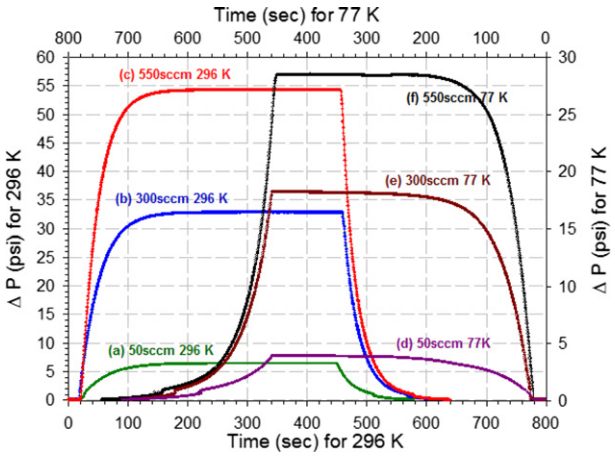

Fig. 7 – The pressure drop ΔP versus time for a neat MOF-5 sample with $D = 0.4732\ g\ cm^{-3}$. The curves (a), (b) and (c) data are taken at 296 K (left & bottom axis), while the curves (d), (e) and (f) data are taken at 77 K (right & top axis) under H_2 flow rate 50 sccm, 300 sccm and 550 sccm, respectively.

increase at 77 K because of the negative thermal expansion coefficient of MOF-5 [12,13]. However, the calculated value of E_a is much higher than the activation energy of surface diffusion of H_2 molecule on sorbents, and further study is in progress.

Using the measured diffusivities, the H_2 diffusion time through the sample can be calculated. The time to reach steady H_2 flow state was plotted in Figs. 7 and 8 for neat MOF-5 and MOF-5 + 5wt.% ENG pellets, respectively. The plots show that the time to reach steady H_2 flow state is almost independent of the H_2 flow rates, which is consistent with data shown in Fig. 2, but it takes slightly longer to reach steady H_2 flow state at 77 K than at 296 K. Fig. 7 shows that a higher density pellet takes significantly longer to reach steady H_2 flow state than the lower density pellet as shown in Fig. 8. This relationship between H_2 diffusion time and pellet density is consistent with the calculated results using Eq. (4). For example, assuming a steady state H_2 flow has been reached when $C(x, t) = 0.99\ C_1$ at 296 K, the estimated time to reach steady state is about 28 s for 0.3010 g cm^{-3} pellets and 569 s for 0.4904 g cm^{-3} pellets, which is in good agreement with the measured time.

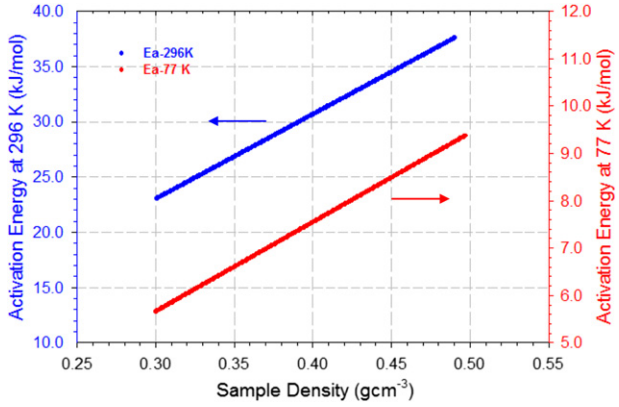

Fig. 6 – Activation energy for hydrogen diffusion through a sample as a function of sample density at 296 K (left axis) and 77 K (right axis).

$$t = \frac{x^2}{4 \times 10^{-4} \times D_f} \approx 28s \text{ to } 569s, \quad x = h = 0.5\ cm$$

The time to reach steady state H_2 flow obtained using Eq. (6) is a conservative approximation for a finite length pellet since H_2 would actually diffuse into the pellet from every surface during H_2 charging in a practical H_2 storage system.

The H_2 diffusivity value can be useful in designing sorbent pelletization by guiding the selection of the shape, size, density, and packaging of the sorbent media within the system. The H_2 transport properties in densified MOF-5 pellets w/o ENG are determined by the microstructure of the pellets, mainly the fraction of the void as represented by pellet density, the size and structures of inner pores in the MOF-5 crystal, the number and distribution of interfaces between MOF-5 and ENG, as well as how those parameters are affected

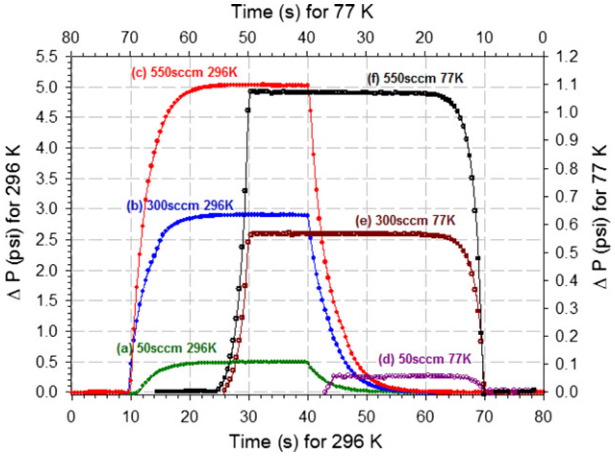

Fig. 8 – The pressure drop ΔP versus time for a neat MOF-5 + 5 wt.% ENG sample with $D = 0.310\ g\ cm^{-3}$. The curves (a), (b) and (c) data are taken at 296 K (left & bottom axis), while the curves (d), (e) and (f) data are taken at 77 K (right & top axis) under H_2 flow rate 50 sccm, 300 sccm and 550 sccm, respectively.

by temperature and hydrogen adsorption. Detailed analyses are still on-going.

4. Conclusion

The hydrogen Darcy permeability and Fick diffusivity of neat MOF-5, MOF-5 + 5 wt.% ENG and MOF-5 + 10 wt.% ENG pellets have been evaluated at 77 K and 296 K. Darcy permeability decreases with increasing pellet density. The Darcy permeability is higher at 296 K than at 77 K. At 296 K, the addition of ENG enhances the H_2 permeability when the pellet density is below 0.4 g cm^{-3} and higher amount of ENG also results in greater H_2 permeability. However, the beneficial effects become less obvious in pellet with a density of above 0.4 g cm^{-3}. The high density MOF-5 pellets lead to inefficient transport of H_2 (low permeability) even though a higher density pellet could have higher volumetric H_2 capacity. At 77 K, the Darcy permeability of MOF-5 samples with and without ENG are nearly the same. The modified compressible Darcy permeability is lower than incompressible Darcy permeability of the same sample. The H_2 diffusivity decreases exponentially with the pellet density at both 77 K and 296 K. Fick's laws of diffusion can be used to characterize the H_2 mass transport through the MOF-5 storage medium, and provide valuable information in selecting the optimal sample geometric shape, dimension, density, and stacking for designing a practical vehicular hydrogen storage system.

Acknowledgments

This work is conducted under US Department of Energy, Office of Energy Efficiency and Renewable Energy, funding grant No. DE-FC36-GO19002. Mr. J. Peterson and Dr. Junsheng Wang are acknowledged for helpful discussions.

REFERENCES

[1] Li J-R, Kuppler RJ, Zhou HC. Selective gas adsorption and separation in metal-organic frameworks. Chemical Society Reviews 2009;38:1477.
[2] Li J-R, Sculley J, Zhou HC. Metal-organic frameworks for separation. Chemical Reviews 2012;112:869.
[3] Li H, Eddaoudi M, O'keeffe M, Yaghi OM. Design and synthesis of an exceptionally stable and highly porous metal-organic framework. Nature 1999;402:276.
[4] Eddaoudi M, Moler DB, Li H, Chen B, Reineke TM, O'Keeffe M, et al. Modular chemistry: secondary building units as a basis for the design of highly porous and robust metal–organic carboxylate frameworks. Accounts of Chemical Research 2001;34:319.
[5] Yang J, Sudik A, Wolverton C, Siegel DJ. High capacity hydrogen storage materials: attributes for automotive applications and techniques for materials discovery. Chemical Society Reviews 2010;39:656.
[6] Rowsell JLC, Millward AR, Park KS, Yaghi OM. Hydrogen storage in functionalized metal-organic frameworks. Journal of the American Chemical Society 2004;126:666.
[7] Hesse M, Mueller U, Yaghi OM. Shaped bodies containing metal-organic frameworks. U.S. Patent 7,524,444 B2, 2009.
[8] Liu D, Purewal JJ, Yang J, Sudik A, Maurer S, Mueller U, et al. MOF-5 composites exhibiting improved thermal conductivity. International Journal of Hydrogen Energy 2012; 37:6109.
[9] Purewal JJ, Liu D, Yang J, Sudik A, Siegel DJ, Maurer S, et al. Increased volumetric hydrogen uptake of MOF-5 by powder densification. International Journal of Hydrogen Energy 2012; 37:2723.
[10] Yun Hang Hu, Lei Zhang. Amorphization of metal-organic framework MOF-5 at unusually low applied pressure. Physical Review B 2010;81:174103.
[11] Müller U, Schubert M, Teich F, Puetter H, Schierle-Arndt K, Pastre J. Metal-organic frameworks - prospective industrial applications. Journal of Materials Chemistry 2006;16:626.
[12] Zhou W, Wu H, Yildirim T, Simpson JR, Hight Walker AR. Origin of the exceptional negative thermal expansion in metal-organic framework-5 Zn_4O(1,4-benzenedicarboxylate)$_3$. Physical Review B 2008;78:054114.
[13] Lock N, Wu Y, Christensen M, Cameron LJ, Peterson VK, Bridgeman AJ, et al. Elucidating negative thermal expansion in MOF-5. Journal of Physical Chemistry C 2010; 114:16181.
[14] Thermohysical Properties of Hydrogen [Internet]. NIST; c2011 [cited 2013 Jan 22]. Available from: http://webbook.nist.gov/cgi/fluid.cgi?ID=C1333740&Action=Page.
[15] Moreira EA, Innocentini MDM, Coury JR. Permeability of ceramic foams to compressible and incompressible flow. Journal of the European Ceramic Society 2004;24:3209.
[16] Shelekhin AB, Dixon AG, Ma YH. Theory of gas diffusion and permeation in inorganic molecular sieve membranes. AIChE Journal 1995;41:58.
[17] Burggraaf AJ. Single gas permeation of thin zeolite (MFI) membranes: theory and analysis of experimental observations. Journal of Membrane Science 1999;155:45.